

Dynamics of Hubbard-band quasiparticles in disordered optical latticesV. W. Scarola¹ and B. DeMarco²¹*Department of Physics, Virginia Tech, Blacksburg, Virginia 24061, USA*²*Department of Physics, University of Illinois at Urbana-Champaign, Urbana, Illinois 61801, USA*

(Received 29 March 2015; revised manuscript received 23 June 2015; published 30 November 2015)

Quantum degenerate gases trapped in optical lattices are ideal test beds for fundamental physics because these systems are tunable, well characterized, and isolated from the environment. Controlled disorder can be introduced to explore suppression of quantum diffusion in the absence of conventional dephasing mechanisms such as phonons, which are unavoidable in experiments on electronic solids. Recent experiments use transport of degenerate Fermi gases in optical lattices [S. S. Kondov *et al.*, *Phys. Rev. Lett.* **114**, 083002 (2015)] to probe extreme regimes. These experiments find evidence for an intriguing insulating phase where quantum diffusion is completely suppressed by strong disorder. Quantitative interpretation of these experiments remains an open problem that requires inclusion of nonzero entropy, strong interaction, and trapping in an Anderson-Hubbard model. We argue that the suppression of transport can be thought of as localization of Hubbard-band quasiparticles. We construct a theory of dynamics of Hubbard-band quasiparticles tailored to trapped optical lattice experiments. We compare the theory directly with center-of-mass transport experiments of Kondov *et al.* with no fitting parameters. The close agreement between theory and experiments shows that the suppression of transport is only partly due to finite-entropy effects. We argue that the complete suppression of transport is consistent with short-time, finite-size precursors of Anderson localization of Hubbard-band quasiparticles. The combination of our theoretical framework and optical lattice experiments offers an important platform for studying localization in isolated many-body quantum systems.

DOI: [10.1103/PhysRevA.92.053628](https://doi.org/10.1103/PhysRevA.92.053628)

PACS number(s): 03.75.Ss, 67.85.-d

I. INTRODUCTION

Understanding the motion of a quantum particle in an otherwise isolated lattice under the influence of an applied field is central to our understanding of conductivity in electronic solids. The theory of Anderson localization [1,2] predicts that quantum diffusion of a single particle can fail in a disordered lattice. Above a critical disorder strength, for which the mobility edge encompasses all states participating in transport [3,4], strong interference forbids quantum diffusion. Anderson's mechanism of localization was first discussed in the context of a simplified model designed to treat the propagation of highly excited states of nuclear spin systems, but it has since been applied to a wide variety of other systems [2], including quantum degenerate atomic gases [5–10]. Disorder-induced localization is also believed to play a key role in metal-insulator transitions in a wide range of materials [2–4].

Subsequent theoretical studies of Anderson localization found that inclusion of realistic effects, specifically interparticle interactions and nonzero temperature [2,11–15], poses prominent problems. The competition between Anderson localization and strong-interaction effects has been studied with a variety of methods, e.g., quantum Monte Carlo [16], dynamical mean-field theory [14,17,18], and related quantum cluster methods [19]. References [14] and [18], for example, found a correlated Anderson insulator ground state for large disorder strengths, indicating that Anderson localization persists in a strongly interacting limit. Other recent work has studied Anderson localization of Bogoliubov quasiparticles in bosonic models [20,21]. A more complete understanding of the interplay of strong interparticle interactions and disorder is urgently needed to enhance our knowledge of strongly correlated materials such as high-temperature superconductors.

Related work by Basko *et al.* [22] has triggered considerable interest in the interplay between interactions, temperature, and Anderson localization. Their work indicates that a correlated Anderson insulator is stable at nonzero temperatures and corresponds to a many-body localized state. This is surprising because one might expect that interactions lead to dephasing effects that mimic the effects of heat and particle number reservoirs [23,24] that are known to lead to conduction via variable range hopping in certain solids [4]. Interactions would be expected to lead to effective reservoirs even in the absence of an explicit reservoir. But Ref. [22] argues, surprisingly, that interactions allow a correlated Anderson insulator to survive up to a characteristic temperature. More recent work (see Ref. [24] for a review) points out that the very notion of temperature should give way to the more general concept of energy density in a many-body localized phase in an isolated quantum system.

Quantum degenerate gases of atoms trapped in optical lattices offer a controlled arena to study the interplay of interactions, disorder, and thermal effects [25–28] because they are, to an excellent approximation, isolated. The entropy per particle, controlled via cooling in a parabolic trap, determines an equilibrium temperature when the lattice is turned on since atomic gases thermalize through interparticle interactions [29–31]. As a result of their isolation, quantum degenerate Fermi gases in optical lattices exhibit quantum diffusion (see, e.g., Ref [32]), even though their temperatures are a significant fraction of the Fermi energy. This offers a useful regime to study because isolated systems can, in principle, exhibit many-body localization even at high energy densities [33]. Furthermore, optical lattice experiments are well characterized [27,34]: interaction strength, lattice depth, entropy, density, and other parameters are all known and tunable. The impact of disorder can therefore be studied

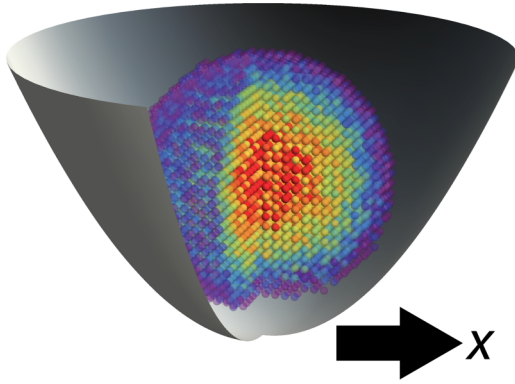


FIG. 1. (Color online) Schematic showing disordered lattice sites in a parabolic trapping potential. The site coloring represents a dense core that gives way to zero density at the edges. The system studied here can be thought of as a strongly interacting high-temperature paramagnet with a density less than 1 at the center. An applied shift of the external trapping potential along the x direction for a time $\tau = \tau_p$ forces center-of-mass motion along the x direction only if the atoms are mobile. τ_p is chosen to be short on the time scale of the inverse trapping frequency.

independently of conventional dephasing phenomena arising from contact with reservoirs [35–42].

Recent experimental work [43] has investigated interacting fermions confined in a cubic optical lattice to study the influence of quenched speckle disorder on center-of-mass transport (Fig. 1). This system is accurately described using the Anderson-Hubbard model, and transport in these experiments is understood to imply the short-time response of the entire system to an applied field [43]. The fact that the entire system responds, and not just states near the Fermi surface, implies an absence of a sharp transition. Nonetheless, the experiments find intriguing insulating behavior above a critical disorder strength that agrees qualitatively with the predictions for many-body localization in the weakly interacting regime [22].

Control over the lattice potential depth and disorder strength was shown to lead to a regime where known types of insulating behavior can be excluded. For example, it was demonstrated that the insulating regime occurs for disorder strengths well below the classical percolation threshold [43]. Furthermore, the system was made dilute enough to avoid forming Mott [44–46] and band insulators. The regime [43] explored, can be thought of as a strongly interacting Hubbard paramagnet with a temperature well below the bandwidth. The insulating behavior of the isolated strongly interacting particles in these experiments [43] is therefore a highly nontrivial probe of localization in many-body quantum states.

In this article, we provide a perspective on disorder-induced localization in the Anderson-Hubbard model and the measurements in Ref. [43]. We establish a connection to Hubbard-band quasiparticles that are very robust because they are stabilized up to energy scales on the order of the interaction energy (as opposed to conventional Landau-Fermi-liquid quasiparticles near Fermi surfaces that set in at a much lower energy scale). We make a direct comparison between theory and experiment with no fitting parameters. This approach enables us to treat the strongly interacting limit, which was not possible using

the perturbation theory employed in Ref. [22]. We derive the equations of motion for the Anderson-Hubbard model in the paramagnetic regime while taking into account all important experimental aspects, particularly trapping and finite-entropy effects. We show that the equations of motion derived here to include a trap reduce to the Hubbard-I [47] approximation normally considered in the translationally invariant limit. This demonstrates that our equations of motion quantitatively capture the dynamics of Hubbard-band quasiparticles in a trap.

We use parameters taken from Ref. [43] to effectively replicate the experiment numerically and find evidence of a quasiparticle mobility edge. We find that at low disorder strengths the Hubbard-band quasiparticles propagate in the lattice under an applied force; that is, they have nonzero mobility. We also study the result of increasing disorder. At large disorder strengths we identify a transition to an insulator through the absence of center-of-mass motion. A direct comparison between theory and experiment shows good agreement. We argue that the insulating behavior observed in Ref. [43] is consistent with short-time, finite-size precursors of Anderson localization of Hubbard-band quasiparticles. To our knowledge, disorder-induced localization in the Hubbard model has not been previously understood using this approach, which is complementary to other methods, e.g., perturbative theory [22] and dynamical mean-field theory [14,17,18].

We begin in Sec. II by defining the model used to simulate the experiments of Ref. [43] and all necessary parameters. Here we also define the center-of-mass velocity as the key observable. In Sec. III we then derive the equations of motion in the paramagnetic regime. Section IV then shows that the equations of motion reduce to the Hubbard-I approximation [47] that was originally used to define Hubbard-band quasiparticles. Here we also show that, in a strongly interacting limit, Hubbard-band quasiparticles obey an effective Anderson model of noninteracting quasiparticles. Section V then defines the approximations used in constructing the initial state that is propagated using the equations of motion. Section VI points out an important feature of the initial states used in these experiments. We find that increasing disorder at fixed entropy effectively raises the system temperature to at most $B/3$, where B is the bandwidth. Even though this heating keeps the temperature well below the bandwidth, it is nonetheless an important aspect of these experiments that must be included to make a quantitative comparison with theory. Section VII presents our central results. Here we directly compare numerical solutions of the equations of motion with experiments. We find that low disorder allows the Hubbard-band quasiparticles to propagate in the trap. But we find a critical disorder strength above which center-of-mass motion is suppressed. We conclude in Sec. VIII by interpreting the results presented here as evidence of the Anderson localization of Hubbard-band quasiparticles.

II. MODEL AND PARAMETER REGIMES

We study the dynamics of an equal population of two-component fermions in a cubic optical lattice in the presence of spatial disorder. For deep lattices we assume that all N particles reside in the lowest Bloch band. In this limit the single-band Anderson-Hubbard model is an excellent

approximation [27,43]:

$$H_{\text{AH}} = \sum_{j,j',\sigma} T_{j,j'} c_{j,\sigma}^\dagger c_{j',\sigma} + U \sum_j n_{j,\uparrow} n_{j,\downarrow} + \sum_j \mu_j n_j. \quad (1)$$

Here $c_{j,\sigma}^\dagger$ creates a fermion of spin $\sigma \in \uparrow, \downarrow$ at a site \mathbf{R}_j , $U > 0$ derives from atomic s -wave scattering, and $n_j = n_{j,\uparrow} + n_{j,\downarrow}$ is the number operator. The matrix elements $T_{j,j'} \equiv -t \delta_{\mathbf{R}_j, \mathbf{R}_{j'+\delta}}$ are written in terms of a Kronecker delta that enforces a hopping energy t between nearest-neighbor sites (δ is a nearest-neighbor bond vector).

The last term in Eq. (1) includes spatially inhomogeneous perturbations to the chemical potential. We define

$$\mu_j = -\mu_0 + \frac{m\omega^2 a^2 R_j^2}{2} + \epsilon_j + V_P \mathbf{R}_j \cdot \hat{x}, \quad (2)$$

where μ_0 is the average chemical potential, m is the atomic mass, ω is the trapping frequency that parameterizes the external confinement, a is the lattice spacing determined by the optical lattice laser wavelength, ϵ_j denotes spatially random disorder, and V_P is a pulse strength that is switched on for a time $\tau = \tau_P$ to effectively shift the trap center.

V_P acts as the analog of a weak electric field used to drive motion along the x direction (see Fig. 1). At long times a single particle with no disorder will oscillate in the trap. But we consider pulse times that are short with respect to the inverse trapping frequency to focus on the regime probed in Ref. [43]. At these short times, the center-of-mass velocity is unidirectional and, in the absence of disorder, increases linearly with V_P .

We consider two distinct distributions of site disorder. In the experiments of Ref. [43] the speckle potential used to establish a disordered optical lattice creates an exponential probability distribution function for the on-site energies [34]:

$$P_E(\epsilon) = \frac{e^{-\epsilon/\Delta_E}}{\Delta_E}, \quad (3)$$

where Δ_E is the strength of the exponentially distributed disorder assuming $\epsilon > 0$ (this is accurate to within 10% of the disorder strength used in Ref. [43]). We also consider a uniform (boxed) disorder probability distribution function for the on-site energies ϵ_j :

$$P_U(\epsilon) = \frac{\Theta(\Delta_U/2 - |\epsilon|)}{\Delta_U}, \quad (4)$$

where Θ is the Heaviside step function and Δ_U parameterizes the strength of the uniformly distributed disorder. P_E introduces behavior that is distinct from more common models with P_U because changing Δ_E at fixed N forces μ_0 to change. This is in contrast to changes in Δ_U which leave μ_0 constant at fixed N .

Equation (1) quantitatively captures the essential properties of the experiments in Ref. [43]. We ignore disorder in t and U that was shown [34] to be narrowly Lorentzian distributed. In what follows, we find that we are able to make a quantitative comparison with experiment even while excluding the disorder in t and U . We will return to this point in Sec. IV.

The experiments proceed by trapping a fixed number of particles with a fixed entropy S . The entropy and all other necessary model parameters were determined in Ref. [43]

TABLE I. Parameters used in the experiments of Ref. [43]. Here the recoil energy is $E_R = \hbar^2/(8ma^2)$, and the atomic species is ^{40}K .

| Lattice depth | V_L | $6E_R$ | $7E_R$ |
|----------------------|------------|----------------------|----------------------|
| Trap frequency | ω | $110 \times 2\pi$ Hz | $114 \times 2\pi$ Hz |
| Lattice spacing | a | 391.1 nm | 391.1 nm |
| Number of particles | N | $47\,100 \pm 6500$ | $48\,700 \pm 1900$ |
| Entropy per particle | S/N | $1.51 \pm 0.18k_B$ | $1.6 \pm 0.17k_B$ |
| Hopping | t | $0.0509E_R$ | $0.0395E_R$ |
| Interaction | U | $0.304E_R$ | $0.355E_R$ |
| Relative strength | U/t | 5.97 | 8.98 |
| Disorder strength | Δ_E | $0-2E_R$ | $0-2E_R$ |
| Pulse time | τ_P | 2 ms | 2 ms |
| Pulse strength | V_P | $0.011E_R$ | $0.011E_R$ |

and are shown in Table I. We focus on the two lattice depths with high U , where $U/t \approx 6$ and $U/t \approx 9$ for $6E_R$ and $7E_R$, respectively, which allows an approximation (the Hubbard-I approximation) that becomes exact in the atomic limit, $t/U = 0$. Table I leaves no fitting parameters in using approximate solutions of Eq. (1) to compare with the experiments of Ref. [43].

We will show that the entropies reported in Table I imply temperatures that are well above the Néel temperature, $\sim t^2/U$ [46,48–52]. The experimentally relevant temperature regimes are above the hopping but below the bandwidth. Our central set of approximations in studying Eq. (1) can be summarized by

$$t \ll U, \quad t \lesssim k_B T < 12t, \quad (5)$$

where the first inequality assumes that we focus on the high-lattice-depth data of Ref. [43] and the second inequality implies that high-temperature limits are valid approximations. Section V shows that the initial state for the parameters defined by Table I can be thought of as a dilute ($\langle n \rangle < 1$) high-temperature paramagnet. We will therefore focus our study on strongly interacting paramagnetic regimes.

To make contact with experimental results presented in Ref. [43] we study the dynamics of the center of mass. The time-dependent center-of-mass velocity in particular,

$$\mathbf{V}_{\text{C.M.}}(\tau) = \sum_j \mathbf{R}_j \langle \dot{n}_j \rangle_D, \quad (6)$$

was inferred from time-of-flight images [43]. Here $\langle \dots \rangle_D$ indicates disorder averaging of expectation values, and τ denotes time. In the following we find that disorder averaging over 25–50 realizations is sufficient to reach convergence in our numerical simulations. We will use Eq. (6) to compute the center-of-mass velocity along the direction of the applied pulse after a time $\tau = \tau_P$:

$$V_{\text{C.M.}} = \hat{x} \cdot \mathbf{V}_{\text{C.M.}}(\tau_P). \quad (7)$$

This quantity is akin to measures of mobility in solids. For example, in the Drude model of electrical conductivity, $V_{\text{C.M.}}$ is proportional to the electron mobility when measured in equilibrium after a pulse. $V_{\text{C.M.}}$ will therefore offer a useful probe to study the impact of disorder on transport of strongly interacting atoms in optical lattices.

III. DYNAMICS FROM EQUATIONS OF MOTION

To study the center-of-mass dynamics we derive equations of motion for correlation functions related to observables. The trapping potential in Eq. (1) breaks translational invariance. We will derive the equations of motion in the site (Wannier) basis as opposed to the more conventional k -space (Bloch) basis to allow studies of local dynamics in trapped lattices. We approximate the equations of motion by relying on the strong-interaction, high-temperature limit, Eqs. (5). The next section shows that our approximation reduces to Hubbard's decoupling of the equations of motion, the Hubbard-I approximation [47], that introduced the concept of Hubbard-band quasiparticles. The equations of motion derived here therefore offer a tool to study the local dynamics of Hubbard-band quasiparticles in the absence of translational invariance.

The exact equations of motion for the charge and spin degrees of freedom are given by

$$i\hbar \frac{d\langle \rho_{l'l}^\sigma \rangle}{d\tau} = \langle [\rho_{l'l}^\sigma, H_{\text{AH}}] \rangle \quad (8)$$

and

$$i\hbar \frac{d\langle \mathbf{S}_{l',l} \rangle}{d\tau} = \langle [\mathbf{S}_{l',l}, H_{\text{AH}}] \rangle, \quad (9)$$

respectively. Here the correlator

$$\rho_{l'l}^\sigma \equiv c_{l',\sigma}^\dagger c_{l,\sigma} \quad (10)$$

is the single-particle density matrix which is off-diagonal in the site indices, l and l' , but measures density along the diagonal since $\rho_{l,l}^\sigma = n_{l,\sigma}$. The spin operator is $\mathbf{S}_{l',l} \equiv \psi_{l'}^\dagger \boldsymbol{\sigma} \psi_l$, where the fermion spinors are $\psi_l^\dagger = (c_{l,\uparrow}^\dagger, c_{l,\downarrow}^\dagger)$ and $\boldsymbol{\sigma}$ are the Pauli matrices. The equations of motion can be generalized to include time dependence in the Hamiltonian, but we exclude that case here.

The high-temperature limit studied here suppresses spin order (which emerges for $k_B T \lesssim t^2/U$). This implies that for an equal number of atoms in each spin state we have a paramagnet:

$$\langle \rho_{l'l}^\uparrow \rangle = \langle \rho_{l'l}^\downarrow \rangle. \quad (11)$$

To focus on the charge degrees of freedom deep in the paramagnetic regime we also assume an absence of in-plane spin order as well. This leads to

$$\langle S_{l'l}^x \rangle = \langle S_{l'l}^y \rangle = \langle S_{l'l}^z \rangle = 0, \quad (12)$$

thus allowing us to focus on approximations of only Eq. (8).

To derive the equations of motion we construct and solve the hierarchy of coupled differential equations with Hubbard's decoupling. The commutator in Eq. (8) can be evaluated:

$$i\hbar \frac{d\langle \rho_{l'l}^\sigma \rangle}{d\tau} = (\mu_{l'} - \mu_l) \langle \rho_{l'l}^\sigma \rangle + U \langle \Gamma_{l'l}^\sigma \rangle + \sum_j [T_{l,j} \langle \rho_{l'j}^\sigma \rangle - T_{l',j} \langle \rho_{jl}^\sigma \rangle], \quad (13)$$

where the U term contains a higher-order correlator:

$$\Gamma_{l'l}^\sigma \equiv \rho_{l'l}^\sigma (n_{l,-\sigma} - n_{l',-\sigma}). \quad (14)$$

The central aim of our protocol is to numerically solve Eq. (13) and use the results to evaluate Eq. (6). This will require an estimate for $\Gamma_{l'l}^\sigma$.

To estimate $\Gamma_{l'l}^\sigma$ we derive the equations of motion for this higher-order correlation function as well. The operator evolves as $d\Gamma_{l'l}^\sigma/d\tau = d\rho_{l'l}^\sigma/d\tau (n_{l,-\sigma} - n_{l',-\sigma}) + \rho_{l'l}^\sigma (dn_{l,-\sigma}/d\tau - dn_{l',-\sigma}/d\tau)$. We use this relation to approximate the evolution of $\langle \Gamma_{l'l}^\sigma \rangle$ by inserting Eq. (13) and decoupling all products of $\Gamma_{l'l}^\sigma$ and $\rho_{l'l}^\sigma$:

$$\begin{aligned} i\hbar \frac{d\langle \Gamma_{l'l}^\sigma \rangle}{d\tau} &= (\mu_{l'} - \mu_l) \langle \Gamma_{l'l}^\sigma \rangle + U \langle \Gamma_{l'l}^\sigma \rangle (n_{l,-\sigma} - n_{l',-\sigma}) \\ &+ \langle n_{l,-\sigma} - n_{l',-\sigma} \rangle \sum_j [T_{l,j} \langle \rho_{l'j}^\sigma \rangle - T_{l',j} \langle \rho_{jl}^\sigma \rangle] \\ &+ \langle \rho_{l'l}^\sigma \rangle \sum_j [T_{l,j} \langle \rho_{lj}^{-\sigma} - \rho_{jl}^{-\sigma} \rangle - T_{l',j} \langle \rho_{l'j}^{-\sigma} - \rho_{j'l}^{-\sigma} \rangle]. \end{aligned} \quad (15)$$

The key decoupling used in deriving this equation is given by a Hartree-Fock-like decoupling in the equations of motion of the form

$$\begin{aligned} \rho_{lj}^{-\sigma} \rho_{l'l}^\sigma &\rightarrow \langle \rho_{lj}^{-\sigma} \rangle \rho_{l'l}^\sigma, \\ n_{l,-\sigma} \Gamma_{l'l}^\sigma &\rightarrow \langle n_{l,-\sigma} \rangle \Gamma_{l'l}^\sigma. \end{aligned} \quad (16)$$

The next section shows that this decoupling reduces to Hubbard's decoupling [47], which has been conventionally implemented in a Green's function approach [47,53].

We self-consistently solve Eqs. (13) and (15) for the time evolution of the correlation functions. We then use the correlation functions to evaluate the center-of-mass position and velocity. One can, in principle, solve for the dynamics at small τ with a linear expansion. But we perform a full self-consistent solution to account for short time scales induced by large disorder strengths and the trap. Large disorder strengths in particular lead to large intersite energy differences and therefore very short intersite tunneling times between certain sites. Our full self-consistent treatment therefore avoids possible problems with a small τ expansion.

The time evolution of other local correlation functions can also be found. For example, the double occupancy $\langle n_{l,\uparrow} n_{l,\downarrow} \rangle$ can be obtained from

$$\begin{aligned} i\hbar \frac{d\langle \gamma_{l'l}^\sigma \rangle}{d\tau} &= (\mu_{l'} - \mu_l) \langle \gamma_{l'l}^\sigma \rangle + \langle \rho_{l'l}^\sigma \rangle \sum_j T_{l,j} [\langle \rho_{lj}^{-\sigma} \rangle - \langle \rho_{jl}^{-\sigma} \rangle] \\ &+ \langle n_{l,-\sigma} \rangle \sum_j [T_{l,j} \langle \rho_{l'j}^\sigma \rangle - T_{l',j} \langle \rho_{jl}^\sigma \rangle] \\ &+ U \langle \gamma_{l'l}^\sigma \rangle (1 - \langle n_{l',-\sigma} \rangle) (1 - \delta_{l,l'}), \end{aligned} \quad (17)$$

where the off-diagonal operator

$$\gamma_{l'l}^\sigma \equiv \rho_{l'l}^\sigma n_{l,-\sigma} \quad (18)$$

captures the conditional hopping of doublons.

IV. CONNECTION TO HUBBARD'S APPROXIMATION

In this section we argue that the formalism we have constructed can be understood in a quasiparticle picture. In strongly interacting systems we often rely on mappings to

weakly interacting quasiparticles to gain a quantitative understanding of otherwise intractable problems. Quasiparticles therefore offer useful tools to probe many-body localization and related phenomena. We can then ask the following question that parallels inquiries into many-body localization of elementary particles: Does spatial disorder localize weakly interacting quasiparticles at nonzero temperature? Here the interactions between the original particles are strong, thus allowing significant dephasing from interactions. But quasiparticle problems are tractable and should therefore allow detailed quantitative studies.

To connect the equations of motion to Hubbard-band quasiparticles we will show that our formalism reduces to Hubbard's approximation in the translationally invariant limit. Our formulation is a local theory designed to incorporate spatial inhomogeneity (i.e., trapping and disorder in the quasiparticle degrees of freedom). By assuming translational invariance we can show that the above formalism simplifies to the equations of motion found from Hubbard's approximation. We first briefly review Hubbard's approximation.

Hubbard's approximation applies the Hartree-Fock decoupling to the equations of motion for the Green's functions. The approximation is, unlike the ordinary Hartree-Fock approximation, exact in both the band limit, i.e., no interactions, and the atomic limit, i.e., infinitely strong interactions. The approximation assumes two Hubbard bands of quasiparticles where the band parameters are renormalized by the density and the interaction. Exact solutions of Hubbard's equations of motion are possible in the translationally invariant limit [$\mu_j \rightarrow -\mu_0$ in Eq. (2)]. The quasiparticle Green's function is

$$G_{k,\sigma}(E) = \frac{\hbar}{E - [\varepsilon(\mathbf{k}) - \mu_0 + \Sigma_\sigma(E)]}, \quad (19)$$

where the nearest-neighbor tunneling leads to the single-particle band dispersion:

$$\varepsilon(\mathbf{k}) \equiv -2t \sum_{v \in x,y,z} \cos(k_v a). \quad (20)$$

The self-energy is [47]

$$\Sigma_\sigma(E) = \frac{U \langle n_{-\sigma} \rangle (E + \mu_0)}{E + \mu_0 - U(1 - \langle n_{-\sigma} \rangle) + i\xi}. \quad (21)$$

Here the density is to be determined self-consistently. $\Sigma_\sigma(E)$ therefore depends on temperature because the density is temperature dependent (see Sec. V). We have also inserted a small number, ξ , which parameterizes the quasiparticle lifetime. Working with a purely real self-energy assumes Hubbard-band quasiparticles with an infinite lifetime. By taking the limit $\xi \rightarrow 0$ it is straightforward to show that $\Sigma_\sigma(E)$ satisfies the Kramers-Kronig relations. We follow the Hubbard-I approximation [47] by setting $\xi = 0$ when we consider the translationally invariant limit. Disorder, included later in a self-consistent numerical protocol, can be parameterized in the Green's function by taking $\xi > 0$.

It is important to note that this decoupling goes beyond conventional Hartree-Fock decouplings of the Hamiltonian [54] (which only capture the dynamics of very weakly interacting limits) to instead apply a decoupling in the equations of motion of higher-order correlation functions. The Hubbard-I approximation reproduces the exact correlation functions of

the Hubbard model in both the weak ($t/U \rightarrow \infty$) and strong ($t/U \rightarrow 0$) interaction limits of the paramagnetic phase. But it breaks down at intermediate interaction strengths, near the Mott transition (half filling), and when magnetic ordering sets in. A review of the limitations of the Hubbard-I approximation can be found in Ref. [55].

Long-lived Hubbard-band quasiparticles are a valid approximation for both the initial state and the short-time dynamics studied here. Section V shows that the initial thermal state produced by the Hubbard-I approximation ($\xi = 0$) reproduces correlation functions obtained from the high-temperature series which therefore shows that the Hubbard-I approximation is valid at these temperatures. It is also reasonable to assume that Hubbard-band quasiparticles are long-lived in the time-propagated state on time scales of the experiment (2 ms). A theory-experiment comparison [56] shows that the absence of dissipation prevents the decay of Hubbard-band quasiparticles, e.g., doublons, because energy-conserving decay processes are higher order in t/U . References [56,57] find doublon lifetimes on the order of $4\hbar/t$, but the transport experiments discussed here [43] are performed on time scales that are more than two orders of magnitude shorter. These comparisons indicate that infinite quasiparticle lifetimes are a reasonable approximation.

We also note that relaxation times in the propagated state are assumed to be dominated by disorder in our calculation. We numerically solve for time-evolved correlation functions in the Hubbard-I approximation in the disordered landscape. Our procedure therefore implicitly imposes a disorder-dominated relaxation time within the Hubbard-I approximation. We rely on the close agreement between theory and experiment to validate this assumption.

Using the self-energy, we can define a spectral density that is useful for calculations:

$$\mathcal{S}_{k,\sigma}(E) = \hbar \delta[E - \varepsilon(\mathbf{k}) + \mu_0 - \Sigma_\sigma(E)]. \quad (22)$$

From the spectral density we find two (Hubbard) bands with spectral weights that depend on the density and interaction. The energies of each band are

$$E_{b,\sigma}(\mathbf{k}) = \frac{U + \varepsilon(\mathbf{k})}{2} + (-1)^b \sqrt{\frac{[U - \varepsilon(\mathbf{k})]^2}{4} + U \langle n_{-\sigma} \rangle \varepsilon(\mathbf{k})},$$

where $b = 1$ ($b = 2$) denotes the lower (upper) Hubbard band. In the limit of weak interaction the bands become degenerate, and we recover the Hartree-Fock limit from Hubbard's approximation.

The Hubbard bands split in the strong interaction limit. To see this we expand $E_{b,\sigma}$ in powers of $1/U$. We find

$$\begin{aligned} E_{1,\sigma} &= [1 - \langle n_{-\sigma} \rangle] \varepsilon(\mathbf{k}) + O(t^2/U), \\ E_{2,\sigma} &= U + \langle n_{-\sigma} \rangle \varepsilon(\mathbf{k}) + O(t^2/U). \end{aligned} \quad (23)$$

This shows that, to lowest order, lower Hubbard-band quasiparticles can be thought of as noninteracting particles but with a renormalized hopping, $t[1 - \langle n_{-\sigma} \rangle]$. (Technically, the renormalized hopping allows the Hubbard-band quasiparticles to interact through the mean field.) The upper Hubbard band is similar but with an energy offset U and a renormalized hopping $t \langle n_{-\sigma} \rangle$. An important aspect of Eq. (23) is that the corrections are $\sim t^2/U$ and are therefore much smaller than the

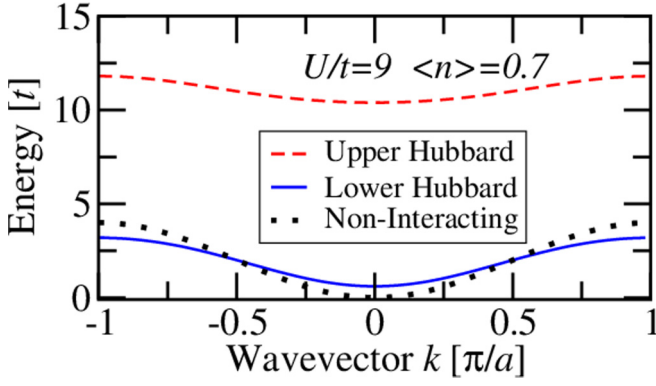


FIG. 2. (Color online) Plot of the energy vs wave vector for a translationally invariant lattice. The solid (dashed) line plots the energy of the lower (upper) Hubbard band $E_{b,\sigma}(\mathbf{k})$ in one dimension. The parameters $U/t = 9$ and $\langle n \rangle = 0.7$ are chosen as being characteristic of the center of the system for the $7E_R$ data in Table I (with $\omega = 0$ and $V_p = 0$). The dotted line plots the noninteracting case, Eq. (20), but in one dimension, for comparison. Here we see that the lower Hubbard band is very similar to the noninteracting band.

temperature in most ongoing optical lattice experiments. Figure 2 plots $E_{b,\sigma}(\mathbf{k})$ in comparison to $\varepsilon(\mathbf{k})$ along one dimension to show that the energetics of Hubbard-band quasiparticles in the lowest band are close to those of free particles.

Hubbard-band quasiparticles are, for $U/t \gg 1$, fundamentally different from quasiparticles near Fermi surfaces normally considered in the Fermi-liquid context. Quasiparticles derived from Fermi surfaces are adiabatically connected to the noninteracting limit. However, Hubbard-band quasiparticles are nonperturbative when viewed from the noninteracting limit because two Hubbard bands with a gap $\sim U$ are assumed. The Hubbard-I approximation becomes exact in the atomic limit. Hubbard quasiparticles therefore have two separate energy scales, a large energy gap $\sim U$ and the energy scale for kinetics t . The limit defined by Eqs. (5) therefore allows a relatively large temperature while maintaining long-lived Hubbard-band quasiparticles that can exhibit quantum diffusion in the absence of dissipation. Conventional quasiparticles, by contrast, decay quickly when the temperature approaches t .

We now show that the formalism presented in Eqs. (13)–(17) reduces to Hubbard’s approximation in the translationally invariant limit. To show this we simplify the equations of motion for $\rho_{l,l'}^\sigma$ and $\gamma_{l,l'}^\sigma$. We can then solve the equations of motion by Fourier transforming into energy and wave-vector variables. We find that the resulting energies are given by $E_{b,\sigma}(\mathbf{k})$.

Equations (13) and (17) define a coupled set of equations that can be solved analytically in the translationally invariant limit. We note that these equations are coupled since $\Gamma_{l,l'}^\sigma = \gamma_{l,l'}^\sigma - \gamma_{l,l'}^{\sigma\dagger}$. We impose translational invariance by setting $\mu_l = \mu_{l'}$. The density then becomes uniform: $\langle n_\sigma \rangle = \langle n_{l,\sigma} \rangle$. We Fourier transform all terms in Eqs. (13) and (17). For example, we set

$$\rho_{\mathbf{k},\mathbf{k}'}^\sigma = N_s^{-1} \sum_{l,l'} e^{-i(\mathbf{k}\cdot\mathbf{R}_l - \mathbf{k}'\cdot\mathbf{R}_{l'})} \rho_{l,l'}^\sigma, \quad (24)$$

where N_s is the number of sites.

We can also transform the coupled set of first-order differential equations in time to a set of coupled algebraic equations by Fourier transforming to energy space. We then find

$$\begin{aligned} -E\rho_{\mathbf{k},\mathbf{k}'}^\sigma &= U(\gamma_{\mathbf{k},\mathbf{k}'}^\sigma - \gamma_{\mathbf{k}',\mathbf{k}}^{\sigma\dagger}) + [\varepsilon(-\mathbf{k}) - \varepsilon(\mathbf{k}')] \rho_{\mathbf{k},\mathbf{k}'}^\sigma, \\ -E\gamma_{\mathbf{k},\mathbf{k}'}^\sigma &= U\gamma_{\mathbf{k},\mathbf{k}'}^\sigma + \langle n_{-\sigma} \rangle [\varepsilon(-\mathbf{k}) - \varepsilon(\mathbf{k}')] \rho_{\mathbf{k},\mathbf{k}'}^\sigma, \end{aligned} \quad (25)$$

where we have dropped higher-order terms, i.e., terms of the form $U\langle n_{-\sigma} \rangle \gamma_{\mathbf{k},\mathbf{k}'}^\sigma$. We have also made use of $T_{l,l'} = N_s^{-1} \sum_{\mathbf{k}} \varepsilon(\mathbf{k}) e^{i\mathbf{k}\cdot(\mathbf{R}_l - \mathbf{R}_{l'})}$.

Equations (25) can be solved analytically for the eigenvalues E by setting $\mathbf{k}' = 0$ and solving for $\rho_{\mathbf{k},0}^\sigma$ and $\gamma_{\mathbf{k},0}^\sigma$. We can, without loss of generality, set $\varepsilon(0) = 0$ in Eq. (25) to make contact with the Hubbard approximation. We find three distinct modes. A trivial high-energy mode with $E = U$ corresponds to a nondispersive doublon mode obtained from solutions with $\rho_{\mathbf{k},0}^\sigma = 0$. But the remaining two modes we find have precisely the same energies as those found in Hubbard’s approximation: $E_{b,\sigma}(\mathbf{k})$. We have therefore shown that the formalism presented in Eqs. (13)–(17) reduces to Hubbard’s approximation in the translationally invariant limit.

The reduction of the dynamics problem posed by Eq. (1) in a high-temperature paramagnetic limit into that of dynamics of Hubbard-band quasiparticles has two important implications. The first is practical: We will be able to compute correlation functions for the initial state using the spectral density. This is discussed in Sec. V.

The second implication is phenomenological. Since the strongly interacting limit can be thought of as nearly free Hubbard-band quasiparticles, the addition of disorder should show features qualitatively similar to a weakly interacting system. We have verified that the quasiparticle picture remains valid even for large disorder strengths, $\Delta_E/t \sim 40$, by checking that the Hubbard-band spectral weight is nonzero. We can therefore construct an effective model of Hubbard-band quasiparticles in a disordered lattice (but in the absence of a trap):

$$H_{\text{eff}} = \sum_{j,j',\sigma,b} \tilde{T}_{j,j'}^{b,\sigma} \tilde{c}_{j,b,\sigma}^\dagger \tilde{c}_{j',b,\sigma} + \sum_{j,b,\sigma} \tilde{\mu}_{j,b,\sigma} \tilde{n}_{j,b,\sigma}, \quad (26)$$

where the tilde indicates quasiparticle operators. $\tilde{\mu}$ is the chemical potential renormalized by the self-energy, and $\tilde{T}_{j,j'}$ indicates quasiparticle hopping with

$$\tilde{T}_{j,j'}^{b,\sigma} = N_s^{-1} \sum_{\mathbf{k}} E_{b,\sigma}(\mathbf{k}) e^{i\mathbf{k}\cdot(\mathbf{R}_j - \mathbf{R}_{j'})}. \quad (27)$$

Here we have assumed that the quasiparticle energies $E_{b,\sigma}(\mathbf{k})$ depend on the Fourier transform of the randomly distributed density.

We can get an intuition for the renormalized hopping if we assume that the density, on average, remains uniform in the presence of disorder. Equations (23) show that in the strongly interacting limit this renormalized hopping reduces to $\tilde{T}_{j,j'}^{1,\sigma} \approx T_{j,j'} \langle 1 - n_{-\sigma} \rangle + O(t^2/U)$ and $\tilde{T}_{j,j'}^{2,\sigma} \approx T_{j,j'} \langle n_{-\sigma} \rangle + O(t^2/U)$ for the lower and upper Hubbard bands, respectively. The renormalized hopping is shown schematically in Fig. 3.

H_{eff} is an effective theory of Hubbard-band quasiparticles that must, in principle, be solved self-consistently. But it

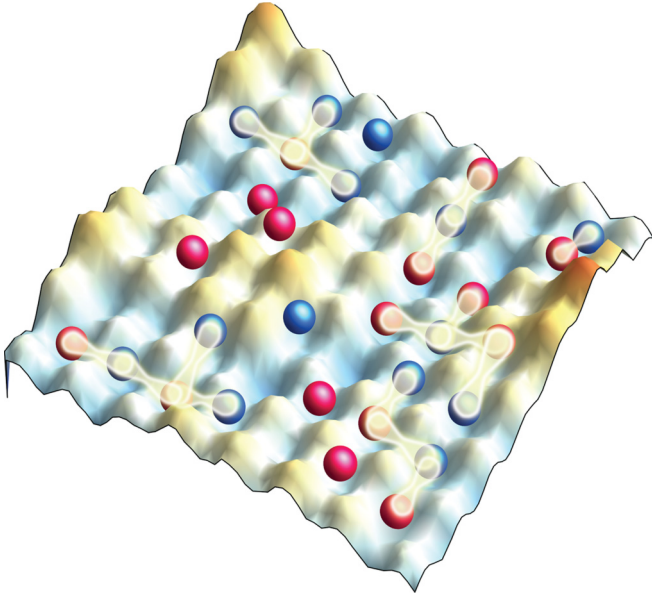


FIG. 3. (Color online) Schematic of one two-dimensional plane of the site-disordered cubic lattice. The blue (dark gray) and red (light gray) spheres depict spin up and down Hubbard-band quasiparticles in the lowest Hubbard band, respectively. The highlighted nearest-neighbor bonds between particles of opposite spin symbolize the renormalized quasiparticle hopping in Eq. (26). The hopping is suppressed on average. For example, a lower-band quasiparticle with spin σ has a renormalized nearest-neighbor hopping $t(1 - n_{-\sigma})$ for large U .

should nonetheless reveal a mobility edge of Hubbard-band quasiparticles because it is essentially a noninteracting Anderson model of Hubbard-band quasiparticles. For example, it is well known that the Anderson model in the cubic lattice with uniform disorder exhibits a mobility edge at $\Delta_U/B = X_c$, where $X_c \approx 1.6$ [58]. For the lower Hubbard band in the absence of a trap and in a paramagnetic state the quasiparticle bandwidth becomes $B = 12t(1 - \langle n \rangle/2)$. H_{eff} therefore qualitatively predicts a mobility edge for Hubbard-band quasiparticles. We will return to this point in discussing the suppression of transport in Sec. VIII.

H_{eff} also shows that ignoring disorder in t and U is justified in the large- U limit. Reference [34] showed that speckle disorder leads to a narrow Lorentzian distribution of t and U . Even though the distribution is narrow, these parameters could, in principle, make significant contributions to dynamics due to the tails of the distribution. But we note that the large- U limit is dominated by dynamics of Hubbard-band quasiparticles (not the original particles). Equations (23) and (26) explicitly show that the effective quasiparticle hopping \tilde{T} and chemical potential $\tilde{\mu}$ are implicitly disordered even if disorder in t and U are excluded. This shows that excluding disorder in t and U still leaves an effective model with all terms disordered. Including disorder in t and U should therefore not qualitatively alter the dynamics of Hubbard-band quasiparticles in the large U limit.

V. INITIAL STATE

To time evolve correlation functions we must accurately establish the initial state. The system evolves in the absence

of a heat or particle number bath. The short-time dependence therefore crucially depends on the initial state. We note that the Hubbard approximation is very accurate in the limit defined by Eqs. (5). To see this we note that the static properties of optical lattice experiments with two-component fermions are also accurately captured by a high-temperature series expansion of Eq. (1) [59–61].

We have checked that the high-temperature series expansion and the Hubbard approximation agree in the limits discussed here [Eqs. (5)]. We have computed correlation functions important for preparing the initial state (density, double occupancy, energy, entropy, and hopping energy) using both the high-temperature series and the Hubbard-I approximation. Both approximations agree in the temperature regime of interest. Figure 4 plots an example comparison for the density. Here we see that all orders of the high-temperature series agree with the Hubbard-I approximation for $T \gtrsim t$. But the agreement breaks down for low T where the high-temperature series fails to provide convergent results and we expect spin correlations to play an important role. In preparing the initial state we have checked that we are working

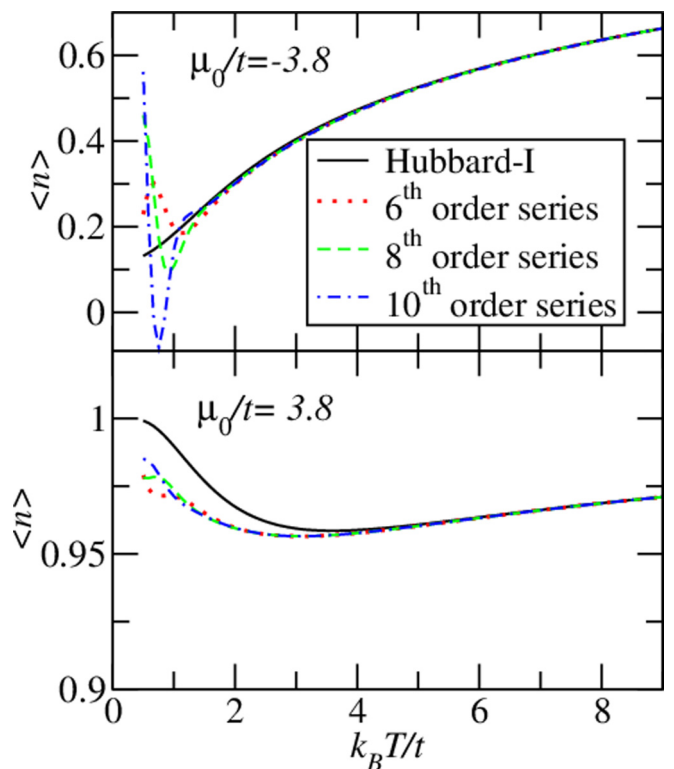


FIG. 4. (Color online) The density of the uniform Hubbard model ($\Delta_U = 0$, $V_P = 0$, and $\omega = 0$) as a function of temperature for $U/t = 9$. Calculations are performed using the high-temperature series and the Hubbard-I approximation for comparison. The high-temperature series is a perturbative expansion of the partition function in powers of $t/k_B T$. Each order corresponds to the largest power in the expansion. The top (bottom) panel shows chemical potentials representative of the edge (center) of the trapped system for the $7E_R$ data in Table I. In both panels we see that agreement for each order of the series breaks down near $k_B T \sim t$, where the Hubbard-I approximation begins to deviate in comparison.

at entropies where the high-temperature series converges and agrees with the Hubbard-I approximation.

In this high- T regime the initial state is also accurately captured by the local-density approximation [53,60]. We take each site as a uniform system and compute correlation functions. In the local-density approximation we assume that each site of the trapped system can be approximated with parameters for a uniform system by setting μ_l to be the chemical potential for the l th uniform system, and we average over all uniform systems. Correlation functions from each site are then combined, and the average chemical potential is determined self-consistently to fix the particle number. In the case of multisite correlation functions a complication arises: the chemical potential varies from site to site. Here we find that nearest-neighbor correlation functions are sufficient to describe the initial state since long-range correlation functions decay quickly at these temperatures. As a result, we are able to approximate two-site correlation functions by setting the chemical potential to be the average between the neighbors.

The local-density approximation was validated in Ref. [60] using two different high-temperature series expansions. In Ref. [60] a series expansion that included the trapping potential was constructed. All terms were included for arbitrary chemical potentials up to order $(t/k_B T)^2$. The expansion with the trapping included was compared with a high-temperature series expansion derived for the uniform limit but with trapping included in the local-density approximation. All correlation functions were found to agree for temperatures high enough to maintain the paramagnet phase. Since the present work examines the same temperature regimes, the local-density approximation is appropriate.

Now that we have validated the Hubbard-I approximation it can be used to approximate the initial state using correlation functions computed directly from the spectral function within the local-density approximation. The spectral theorem implies that we can compute the initial ($\tau = 0$) correlation function for $\rho_{l'l}^\sigma$ using

$$\langle \rho_{l'l}^\sigma \rangle(\tau = 0) = \sum_k \frac{e^{-i(\mathbf{R}_{l'} - \mathbf{R}_l) \cdot \mathbf{k}}}{2\hbar N_s} \int_{-\infty}^{\infty} dE f(E) \times \mathcal{S}_{k,\sigma}(E - \bar{\mu}), \quad (28)$$

where $\bar{\mu} \equiv (\mu_l - \mu_{l'})/2$ and $f(E)$ is the Fermi-Dirac distribution function. Here we assume $\langle \rho_{l'l}^\sigma \rangle$ is equal to its Hermitian conjugate. A similar relation can be used to obtain $\Gamma_{l'l}^\sigma$ as well:

$$\langle \rho_{l'l}^\sigma n_{l,-\sigma} \rangle(\tau = 0) = \sum_k \frac{e^{-i(\mathbf{R}_{l'} - \mathbf{R}_l) \cdot \mathbf{k}}}{2\hbar N_s} \int_{-\infty}^{\infty} dE f(E) \times \left[\frac{E - \varepsilon(\mathbf{k})}{U} \right] \mathcal{S}_{k,\sigma}(E - \bar{\mu}). \quad (29)$$

Using these relations we are able to set the initial-state correlation functions with a protocol discussed in Sec. VII. The protocol allows the use of the Hubbard approximation to compute initial-state correlation functions at fixed entropy for a given disorder configuration. The following discusses the temperature dependence in the initial state in the presence of disorder.

VI. ADIABATIC HEATING DUE TO DISORDER IN THE INITIAL STATE

The temperature in ultracold-atom experiments is determined by the entropy. The relationship between temperature and entropy relies, in general, on the intricate interplay between kinetics and interactions. The addition of disorder adds another complication that alters the entropy-temperature relation. Below we show that the addition of disorder leads to adiabatic heating in the initial state. Specifically, we find that, at fixed entropy, increasing disorder increases the temperature. This observation has important consequences for the interpretation of the data in Ref. [43] and other optical lattice experiments because increasing disorder strengths also increases temperature. In subsequent sections we take adiabatic heating from disorder into account when preparing the initial state in a trap.

We use the high-temperature series expansion to show that the paramagnet experiences adiabatic heating due to disorder. The solid line in Fig. 5 shows an example of the entropy per particle versus temperature for an initial state without a trap.

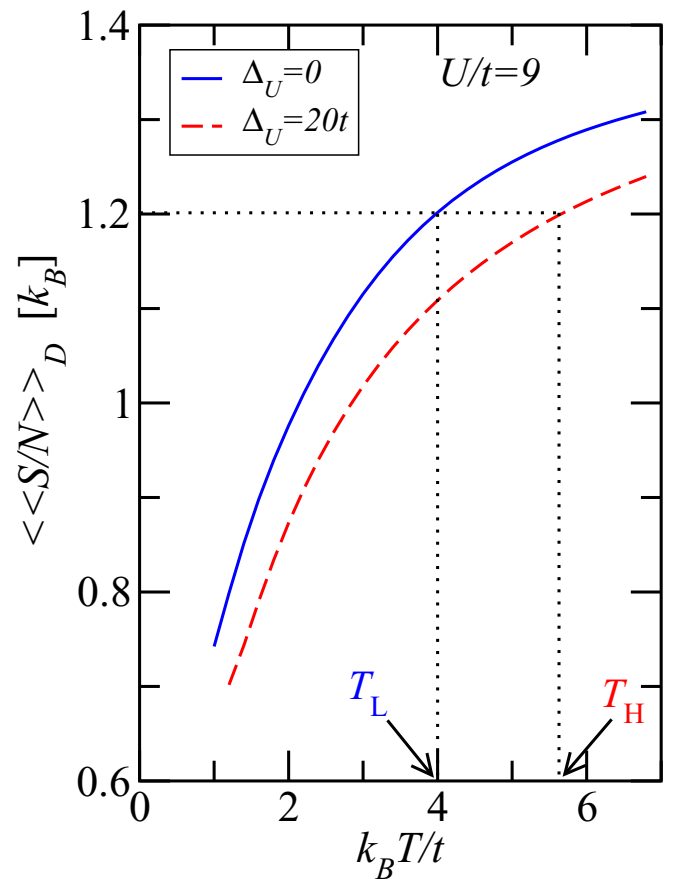


FIG. 5. (Color online) The disorder-averaged entropy per particle computed as a function of temperature for Eq. (1) in the absence of a trapping potential or a pulse ($\omega = 0$ and $V_p = 0$). The horizontal dotted line indicates a fixed entropy per particle, $S/N = 1.2k_B$. The solid (dashed) lines were computed using $\Delta_U = 0$ ($\Delta_U = 20t$) and $\mu_0/t = 3.8$. The vertical lines labeled with T_L and T_H point to low and high temperatures, respectively. The entropy-temperature curve with a high disorder leads to a higher temperature.

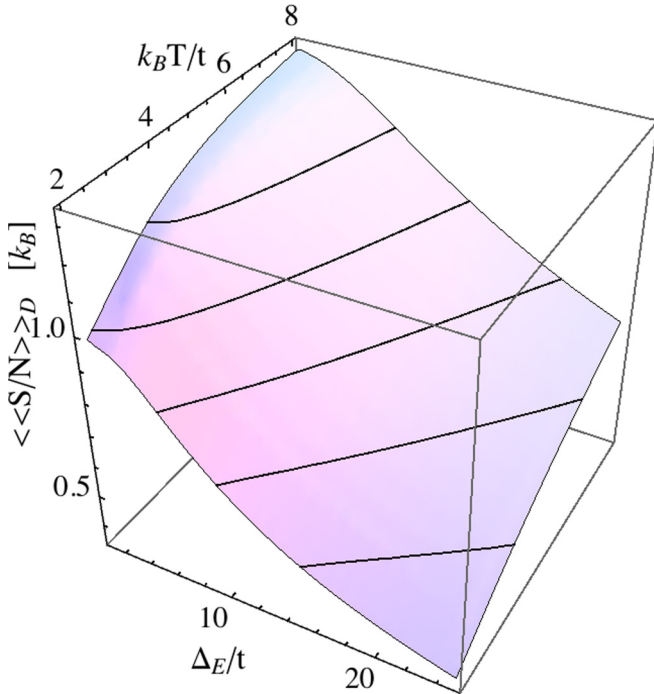


FIG. 6. (Color online) Disorder-averaged entropy per particle plotted as function of both temperature and disorder strength for Eq. (1) in the absence of a trapping potential or an applied force ($\omega = 0$ and $V_p = 0$). The eighth-order high-temperature series expansion was used within the local-density approximation. $U/t = 9$ and $\mu_0/t = 3.8$ were chosen as being characteristic of the center of the system for the $7E_R$ data in Table I. The black contour lines indicate adiabats that reveal significant adiabatic heating due to increasing exponential disorder.

We set $\mu_0/t = 3.8$ because it characterizes the nondisordered limit of experiments reported in Ref [43]. We find $\langle n \rangle < 1$. Here we see that a fixed entropy (horizontal dotted line) sets a low temperature, T_L , in the absence of disorder. Because optical lattice experiments take place in the absence of a heat bath, entropy is preserved when a disordered optical lattice is applied to a trapped gas. We then include a disorder strength $\Delta_U = 20t$ in a calculation of the entropy per particle. We use the local-density approximation and integrate over disorder configurations [see Eqs. (A3)]. The dashed line shows the disorder-averaged results. The entropy is significantly lower. The system therefore acquires a higher temperature, T_H , at the same entropy.

Adiabatic heating due to disorder arises because increasing the disorder strength in a single band reduces the number of available states. As a result the entropy (which is the logarithm of the number of available states) decreases with increasing disorder. The net effect is then an increase in temperature if the entropy is required to be fixed while increasing disorder.

Adiabatic heating becomes more pronounced with exponentially distributed disorder. Figure 6 plots the entropy per particle as a function of both exponential disorder strength and temperature. The black lines depict adiabats. The corresponding temperature can therefore increase by as much as a factor of 2 at fixed entropy over the range of disorder strengths considered here. The impact of adiabatic heating due

to disorder on center-of-mass dynamics in trapped systems is discussed in more detail in the following sections.

VII. CENTER-OF-MASS DYNAMICS: COMPARISON WITH EXPERIMENT

This section culminates in a direct comparison between results from the equations of motion and experiments. We find that small-system-size simulations can be scaled to directly compare with experiments with no fitting parameters. The close comparison between experiment and theory shows that we can interpret the experiments of Ref. [43] as motion of Hubbard-band quasiparticles. The simulations and experiments are consistent with finite-size precursors of Anderson localization of Hubbard-band quasiparticles.

We now use Eqs. (28) and (29) to compare with experiments in Ref. [43] using experimental input parameters from Table I. To use our formalism to compute the center-of-mass dynamics we prepare an initial state at fixed entropy in a disordered landscape. The system is numerically time evolved. The center-of-mass velocity is computed at the pulse time and then disorder averaged. These simulations are performed on system sizes up to $L = 11$, with $L = L_x = L_y = L_z$. Finite-size extrapolation is performed by decreasing the trap frequency and repeating the simulation for large system sizes while keeping μ_0 fixed to values found for experimentally relevant system parameters.

To keep the pulse time short on the time scales of the trapping frequency (as is done experimentally [43]) we have to rescale the pulse time used in our simulations. The pulse time at system size L , τ_L , is adjusted for each trap frequency at system size L , ω_L , to maintain $\tau_L = \tau_P \sqrt{\omega/\omega_L}$. This allows a scaling to the trapping frequency and the pulse time found in Table I, ω and τ_P , respectively. The impulse formula (Appendix A) shows that this establishes an $\omega_L^{-1/2}$ scaling of $V_{C.M.}$. This scaling is expected since the center-of-mass velocity from the impulse formula scales as $V_0 \sim \tau_L \sim \omega_L^{-1/2}$ (Appendix A). We have checked below that our finite-size extrapolations do scale as $\omega_L^{-1/2}$, as expected.

We use the following protocol to prepare initial states: (1) We choose an entropy per particle determined experimentally, high trap frequency (chosen to trap the system within the finite-size limitations of our simulations), and a small number of particles. (2) We choose a random distribution of chemical potentials according to Eq. (3). (3) We then self-consistently adjust μ_0 and T so that the particle number and entropy match the values set in step 1. This is done using the high-temperature series expansion in the local-density approximation. The series expansion is controlled at these temperatures because we can check higher orders [60,61]. We find that eighth order in the expansion is sufficient for parameters considered here. The Hubbard approximation gives identical results for thermodynamic functions. (4) We then use Eqs. (28) and (29) to compute the initial-state correlation functions. (5) We then return to step 1 to repeat the process with a smaller trap frequency.

We find that adiabatic heating in the initial state increases the temperature by no more than a factor of 2. For all system sizes studied we find that the temperature remains

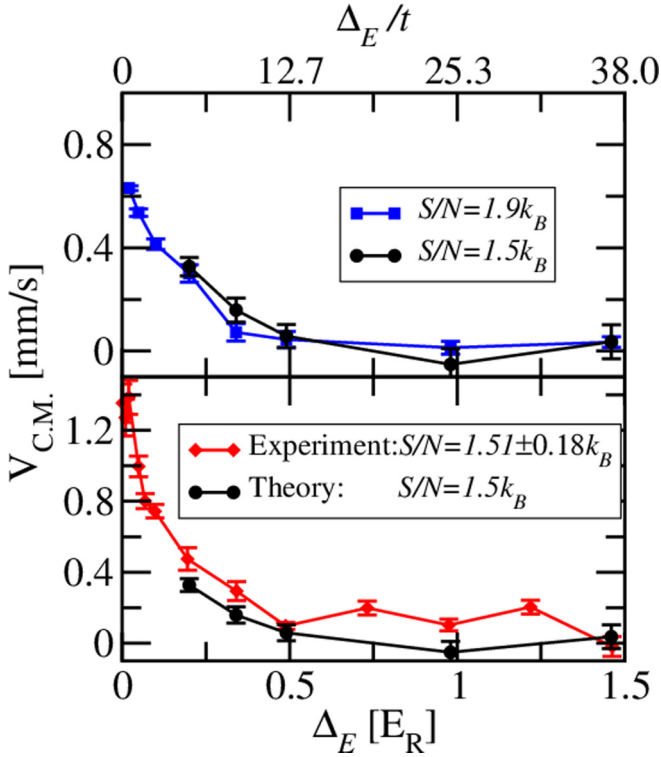


FIG. 7. (Color online) (top) Disorder-averaged center-of-mass velocity as a function of the disorder strength for two different entropies. Here the initial-state correlation functions are estimated in the local-density approximation [using Eqs. (28) and (29) in combination with a high-temperature series expansion] and time evolved in the trap [using Eqs. (13) and (15)]. Model parameters are taken from the $6E_R$ data in Table I. The $S/N = 1.5k_B$ results are plotted only for large disorder strengths because here adiabatic heating allows access to temperatures high enough to be consistent with the approximations made in preparing the initial state. (bottom) The circles plot the same information as the top panel, and the diamonds plot experimental data from Ref. [43] for comparison. The lines are a guide to the eye. The error bars on the numerical simulations are the standard error found from disorder averaging, while the experimental error bars are the standard error in the mean for seven to nine measurements averaged for each point.

nearly constant as a function of system size. At the largest disorder strengths, $\Delta_E \sim 1.5E_R$, we still find $k_B T < 4t$. We conclude that adiabatic heating increases the temperature, but the temperature is still well below the bandwidth, $12t$.

Given the initial state, we numerically time evolve correlation functions according to Eqs. (13) and (15), extrapolate to the thermodynamic limit, and disorder average. Figures 7 and 8 plot $V_{C.M.}$ versus disorder strength for the $6E_R$ and the $7E_R$ parameters, respectively. The data result from time evolving the initial correlators, Eqs. (28) and (29). The top panels show results for two different entropies. The larger entropy leads to temperatures with $T \gtrsim t$. The approximations made here (paramagnetic order, no spin correlations, and the local-density approximation) are therefore valid at all disorder strengths for the higher entropy. The top panels also compare low-entropy data that are consistent with the entropies used in experiments (see Table I). Here adiabatic heating increases

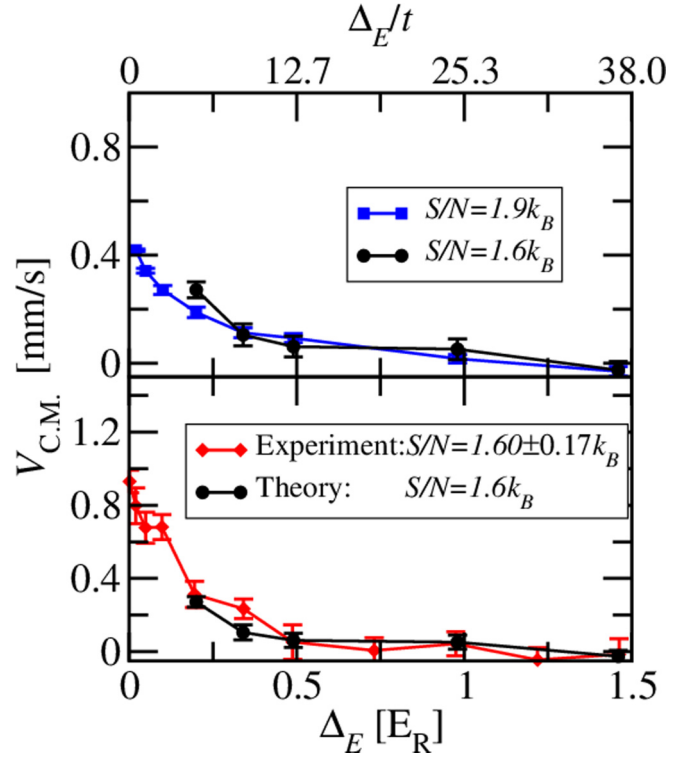


FIG. 8. (Color online) The same as Fig. 7, but for the $7E_R$ data in Table I. Here the comparison between theory and experiment is better because U/t is larger.

the temperature to $T \gtrsim t$ only for $\Delta_E \gtrsim 0.2E_R$. Below these disorder strengths the approximations made here break down because the temperatures are low enough to introduce poles in thermodynamic functions using either the high-temperature series expansion (even out to tenth order) or the Hubbard approximation.

The top panels of Figs. 7 and 8 clearly show a suppression of the center-of-mass velocity with disorder. The mapping to Hubbard-band quasiparticles in the lowest Hubbard band allows delineation of the sources of the suppression: (1) As exponentially distributed disorder is increased, the bias in the distribution leads to more sites with higher densities. The increase in average density slows the propagation of the Hubbard-band quasiparticles because the renormalized tunneling is given by $t(1 - n/2)$. This effect was implicit in the suppression shown in Appendix A (see Fig. 9). We find that this is a weak effect because the system is dilute, i.e., $\langle n_j \rangle / 2 \ll 1$ for many sites (the edges make up about 1/3 of the system). (2) Adiabatic heating due to disorder also suppresses $V_{C.M.}$. The increase in the resulting temperature lowers the nearest-neighbor correlations, e.g., $\langle \rho_{i,i+1}^\sigma \rangle$, inherent in the initial state. The initial state is therefore slower to respond because $V_{C.M.}$ scales linearly with terms like $t \langle \rho_{i,i+1}^\sigma \rangle$. This effect was shown to dominate only at lower disorder in Appendix B (see Fig. 10). Furthermore, we find that the temperature is at most $B/3$ at the largest disorder strength, $\Delta_E \sim 1.5E_R$. (3) These effects are modest and are not sufficient to completely localize the center of mass. The final effect derives from disorder-induced scattering. The presence of disorder lowers the localization length so that propagation is

impossible for $\Delta_E > 0.5E_R$. This final effect is consistent with a finite-size precursor of Anderson localization of Hubbard-band quasiparticles because the critical disorder strength, $\Delta_E \approx 0.5E_R$, is near the approximate location expected for the Anderson metal-insulator transition, near $B \approx 0.47E_R$.

The bottom panels in Figs. 7 and 8 show a comparison between the results obtained from our formalism and the experimental data of Ref. [43]. The comparison is made where possible (in the high-temperature regime). The agreement in Fig. 8 is better because U is larger. The Hubbard approximation becomes exact in the atomic limit. The comparison suggests that the data from Ref. [43] can be thought of as revealing a mobility edge of Hubbard-band quasiparticles.

VIII. DISCUSSION

We have found that two-component fermions in an optical lattice fail to respond to a force for sufficiently strong disorder, implying a phenomenon reminiscent of Anderson localization in bulk systems. At strong disorder strengths the atoms fail to move under weak perturbations. Here the suppression of quantum diffusion indicates that the assumption of a thermal initial state is incorrect, i.e., that the system is inherently non-ergodic at large disorder strengths. Our comparison between theory and experiment is therefore consistent with Anderson localization of Hubbard-band quasiparticles at large disorder strengths but a mobile state of Hubbard-band quasiparticles at low disorder strengths. We interpret these results as evidence of a mobility edge of Hubbard-band quasiparticles.

We can compare the center-of-mass velocity studied here with conductivity studied in solids. Both measures can be used as diagnostics of localization. The dc conductivity in solids is typically defined in infinite system sizes while in equilibrium. The dc conductivity therefore gives a long-time, large-length-scale probe of the single-particle density matrix. The center-of-mass velocity is proportional to mobility and therefore also offers an equivalent probe of the single-particle density matrix provided the system is infinitely large and it is allowed to evolve indefinitely. But the center-of-mass velocity studied here was considered on time scales inversely proportional to the trap frequency and in finite system sizes out of equilibrium. We therefore conclude that the results presented in Figs. 7 and 8 offer only a short-time, finite-size estimate for the conductivity.

Our work opens interesting directions for future studies of localization physics with Hubbard-band quasiparticles. The work presented here is consistent with quantum Monte Carlo results [16] and dynamical mean-field theory studies of the Anderson-Hubbard model [14,17,18]. But these methods could be used to tackle lower temperature limits and include spin fluctuations in a comparison with low-temperature experiments.

Furthermore, future work will be needed to rigorously establish a connection between the localized state found here and many-body localization. The suppression of transport discussed here is a necessary condition for many-body localization. But future work should look at sufficient conditions for many-body localization using, e.g., entanglement measures in the Anderson-Hubbard model to make a direct comparison with experiments.

Note added. Recently, we became aware of work in Ref. [62] that compared the entanglement entropy with population imbalance in incommensurate optical lattices.

ACKNOWLEDGMENTS

V.W.S. acknowledges support from United States Air Force Office of Scientific Research under Grant No. FA9550-11-1-0313. B.D. acknowledges support from the National Science Foundation under Grant No. PHY12-05548 and from the Army Research Office under Grant No. W9112-1-0462.

APPENDIX A: ORDER OF MAGNITUDE ESTIMATE

This appendix uses a semiclassical impulse formula for Hubbard-band quasiparticles to estimate the center-of-mass velocity dependence on disorder strength for very weak disorder. This estimate shows that renormalization of the quasiparticle hopping due to disorder can suppress the center-of-mass velocity. It also yields the correct order of magnitude for the center-of-mass velocity at low disorder. A simple order of magnitude estimate for the center-of-mass velocity will

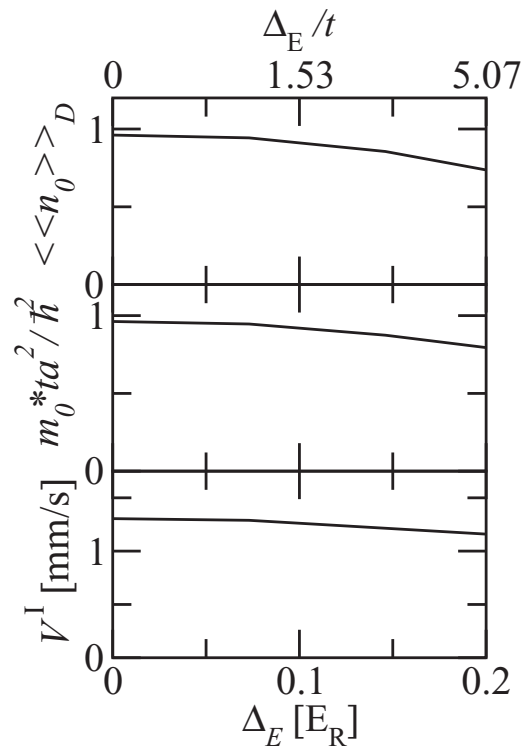


FIG. 9. The top and middle panels plot the density and the quasiparticle effective mass, Eq. (A1), respectively, as a function of disorder strength for a chemical potential at the central site. The bottom panel plots the center-of-mass velocity vs disorder strength from a disorder-averaged impulse formula, Eq. (A2), that estimates the velocity of Hubbard-band quasiparticles in the trap size consistent with experiment. The local-density approximation was used to sum over all sites. All quantities are computed using the high-temperature series expansion at eighth order with the parameters chosen from the $7E_R$ data in Table I but with $S/N = 1.9k_B$. Equations (A3) were used as rough estimates for disorder averaging.

be useful in establishing a scaling relation to extrapolate our finite-sized simulations to experimental system sizes.

To estimate the center-of-mass velocity we use a semiclassical estimate of velocities in combination with the local-density and effective-mass approximations. The quasiparticle effective mass in the lowest Hubbard band is obtained from the single-particle effective mass using the replacement $t \rightarrow t(1 - n_j/2)$:

$$m_j^* = \frac{\hbar^2}{2t(1 - \langle n_j \rangle_D/2)a^2}, \quad (\text{A1})$$

where the limit $\langle n_j \rangle \rightarrow 0$ returns the single-particle effective mass. Note that disorder averaging is implicit in this definition.

At short times, the semiclassical estimate of the center-of-mass velocity reduces to the well-known impulse formula. We apply the impulse formula to the dynamics of Hubbard-band quasiparticles in the lowest band. (Note that the impulse formula also follows from the generalized Kohn's theorem in an effective-mass approximation.) Averaging the velocity of each site $\langle \dot{R}_j^x \rangle$ leads to a total center-of-mass velocity for one disorder configuration, $N^{-1} \sum_j^{N_s} \langle n_j \rangle \langle \dot{R}_j^x \rangle$. Applying the impulse formula to Hubbard-band quasiparticles and averaging over disorder realizations give an approximation of the center-of-mass velocity:

$$V^1 = V_0 \left[1 - \sum_j^{N_s} \langle (n_j)^2 \rangle_D / (2N) \right], \quad (\text{A2})$$

where $V_0 \equiv 2aV_P\tau_{Pt}/\hbar^2$ depends linearly on τ_P and $\langle (n_j)^2 \rangle_D$ indicates the disorder average of $\langle n_j \rangle^2$.

V^1 gives the correct order of magnitude for the center-of-mass velocity. To show this we use the high-temperature series expansion to estimate the density in the initial state in the trap. We choose the parameters for the $7E_R$ lattice depth presented in Table I, but we fix the entropy to be $S = 1.9k_B$.

We use a simplified version of the protocol constructed in the main text to get a rough estimate of V^1 . Once the entropy and particle number are fixed, the approach used in the main text then finds μ_0 and T at each disorder configuration using the high-temperature series expansion. These parameters are then, for each disorder configuration, used to compute $\langle n_j \rangle$ within the trap. Disorder averaging proceeds by summing the center-of-mass velocity over all disorder configurations. But in this appendix we solve for the chemical potential and temperature differently so that we can access experimentally relevant system sizes without finite-size extrapolation. We use the high-temperature series expansion to approximate the entropy and density with integration (rather than explicit summation) over the disorder distribution:

$$\begin{aligned} \langle \langle S \rangle \rangle_D &\approx \int_0^\infty d\epsilon P_E(\epsilon) S(\epsilon), \\ \langle \langle n \rangle \rangle_D &\approx \int_0^\infty d\epsilon P_E(\epsilon) \langle n(\epsilon) \rangle. \end{aligned} \quad (\text{A3})$$

These approximations can be used to self-consistently solve for T and μ_0 given S and N for large system sizes. This simplified protocol uses entropies and densities that are not self-consistently solved for each disorder configuration but are instead taken in a mean-field limit separately. As a

result, self-consistent solutions of these coupled formulas offer only a rough estimate for T and μ_0 because they are assumed to decouple for each disorder configuration. We can therefore apply these approximations only for low disorder strengths.

The top panel of Fig. 9 plots the disorder-averaged density of the central site in the trap as a function of disorder strength. Here we see that the density decreases due to adiabatic heating and a redistribution of the particles due to biased exponential disorder. The quasiparticle effective mass (middle panel) therefore also decreases.

The bottom panel of Fig. 9 plots the disorder-averaged center-of-mass velocity from Eq. (A2). Here we see that the velocity decreases due to an enhancement of the density. The experimental data, for comparison, starts out with a center-of-mass velocity ~ 1 mm/s. The impulse formula for Hubbard-band quasiparticles therefore gives the correct order of magnitude and shows suppression due to a modulation of the density due to disorder.

APPENDIX B: TEMPERATURE DEPENDENCE

In this appendix we study the temperature dependence of the center-of-mass velocity in small trapped systems by solving for the dynamics of correlators using Eqs. (13) and (15). Here it is shown that temperature increases (expected in adiabatic heating) suppress the center-of-mass velocity but only for low disorder strengths.

We can use Eqs. (13) and (15) to compute the center-of-mass dynamics in trapped systems on small system sizes. We solve Eqs. (13) and (15) numerically. The initial state is determined using Eqs. (28) and (29) within the local-density approximation at fixed temperature. Figure 10 shows example

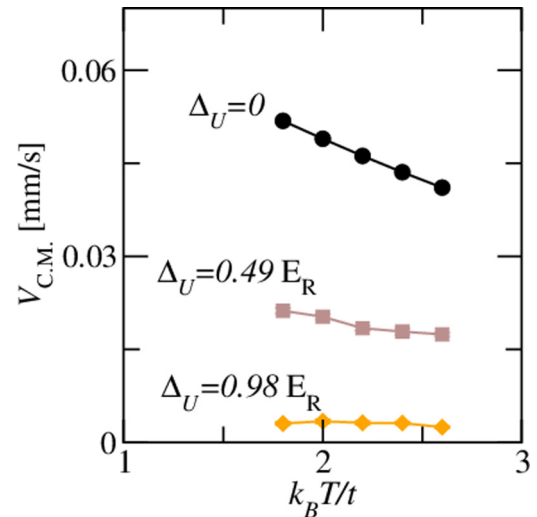


FIG. 10. (Color online) The disorder-averaged center-of-mass velocity [Eq. (7)] as a function of temperature for several disorder strengths computed from solutions of Eqs. (13) and (15). Parameters are chosen to yield a small system-size replica of the larger system implied by the parameters for the $7E_R$ data in Table I (see text). The velocities are disorder averaged using uniform disorder. Here we see that increasing temperature suppresses the velocity only at low disorder strengths.

results for the center-of-mass velocity. The simulations are carried out on a periodic cubic lattice with edges of size $L = 11$, where the trap zeros the density at the edges. We consider a small-system-size replica of larger experimental parameters by choosing a stronger trap frequency $\hbar\omega/t = 0.757$ but at the same chemical potential as that found for experimental system sizes, $\mu_0/t = 3.8$. $\tau_P = 0.514h/t$ is chosen by a trap-dependent rescaling discussed in Sec. VII. The entropy is allowed to vary, but otherwise, the remaining parameters are chosen from the $7E_R$ data in Table I.

Figure 10 shows that by increasing temperature, the center-of-mass velocity can decrease at low disorder. This is the opposite of what is expected from variable-range hopping in common regimes, e.g., in semiconductors, where the presence

of a bath typically increases conductivity with increasing temperature. Here we do not have an external bath. At low disorder, increasing temperature suppresses the amplitude for particles to tunnel between neighboring sites, e.g., $t\langle\rho_{i,t+1}^\sigma\rangle$, in the initial state. As a result, the center-of-mass velocity (which scales linearly with the nearest-neighbor elements of the single-particle density matrix) is suppressed with increasing temperature. The high disorder limit has a different behavior. Here the dynamics is strongly suppressed by disorder, and the thermal suppression of tunneling has little effect. These qualitative trends show that, when we study the experimentally relevant fixed entropy case, adiabatic heating due to disorder will tend to suppress the center-of-mass velocity only at low disorder strengths.

-
- [1] P. W. Anderson, Absence of diffusion in certain random lattices, *Phys. Rev.* **109**, 1492 (1958).
- [2] *50 Years of Anderson Localization*, edited by E. Abrahams (World Scientific, Singapore, 2010).
- [3] N. Mott, *Metal Insulator Transitions* (Taylor and Francis, London, 1974).
- [4] N. Mott, The mobility edge since 1967, *J. Phys. C* **20**, 3075 (1987).
- [5] J. Billy, V. Josse, Z. Zuo, A. Bernard, B. Hambrecht, P. Lugan, D. Clément, L. Sanchez-Palencia, P. Bouyer, and A. Aspect, Direct observation of Anderson localization of matter waves in a controlled disorder, *Nature (London)* **453**, 891 (2008).
- [6] G. Roati, C. D’Errico, L. Fallani, M. Fattori, C. Fort, M. Zaccanti, G. Modugno, M. Modugno, and M. Inguscio, Anderson localization of matter waves in a Bose-Einstein condensate, *Nature (London)* **453**, 895 (2008).
- [7] J. Chabé, G. Lemarié, B. Grémaud, D. Delande, P. Szriftgiser, and J. C. Garreau, Experimental Observation of the Anderson Metal-Insulator Transition with Atomic Matter Waves, *Phys. Rev. Lett.* **101**, 255702 (2008).
- [8] G. Lemarié, J. Chabé, P. Szriftgiser, J. C. Garreau, B. Grémaud, and D. Delande, Observation of the Anderson metal-insulator transition with atomic matter waves: Theory and experiment, *Phys. Rev. A* **80**, 043626 (2009).
- [9] S. S. Kondov, W. R. McGehee, J. J. Zirbel, and B. DeMarco, Three-dimensional Anderson localization of ultracold matter, *Science* **334**, 66 (2011).
- [10] F. Jendrzejewski, A. Bernard, K. Müller, P. Cheinet, V. Josse, M. Piraud, L. Pezze, L. Sanchez-Palencia, A. Aspect, and P. Bouyer, Three-dimensional localization of ultracold atoms in an optical disordered potential, *Nat. Phys.* **8**, 398 (2012).
- [11] A. M. Finkel’shtein, Influence of Coulomb interaction on the properties of disordered metals, *Zh. Eksp. Teor. Fiz.* **84**, 168 (1983).
- [12] P. A. Lee and T. V. Ramakrishnan, Disordered electronic systems, *Rev. Mod. Phys.* **57**, 287 (1985).
- [13] T. Vojta, F. Epperlein, and M. Schreiber, Do Interactions Increase or Reduce the Conductance of Disordered Electrons? It Depends!, *Phys. Rev. Lett.* **81**, 4212 (1998).
- [14] K. Byczuk, W. Hofstetter, and D. Vollhardt, Mott-Hubbard Transition vs. Anderson Localization of Correlated, Disordered Electrons, *Phys. Rev. Lett.* **94**, 056404 (2005).
- [15] F. Evers and A. Mirlin, Anderson transitions, *Rev. Mod. Phys.* **80**, 1355 (2008).
- [16] P. J. H. Denteneer, R. T. Scalettar, and N. Trivedi, Conducting Phase in the Two-Dimensional Disordered Hubbard Model, *Phys. Rev. Lett.* **83**, 4610 (1999).
- [17] A. Georges, G. Kotliar, W. Krauth, and M. J. Rozenberg, Dynamical mean-field theory of strongly correlated fermion systems and the limit of infinite dimensions, *Rev. Mod. Phys.* **68**, 13 (1996).
- [18] D. Semmler, J. Wernsdorfer, U. Bissbort, K. Byczuk, and W. Hofstetter, Localization of correlated fermions in optical lattices with speckle disorder, *Phys. Rev. B* **82**, 235115 (2010).
- [19] T. Maier, M. Jarrell, T. Pruschke, and M. Hettler, Quantum cluster theories, *Rev. Mod. Phys.* **77**, 1027 (2005).
- [20] P. Lugan, D. Clément, P. Bouyer, A. Aspect, and L. Sanchez-Palencia, Anderson Localization of Bogolyubov Quasiparticles in Interacting Bose-Einstein Condensates, *Phys. Rev. Lett.* **99**, 180402 (2007).
- [21] P. Lugan and L. Sanchez-Palencia, Localization of Bogoliubov quasiparticles in interacting Bose gases with correlated disorder, *Phys. Rev. A* **84**, 013612 (2011).
- [22] D. M. Basko, I. L. Aleiner, and B. L. Altshuler, Metal-insulator transition in a weakly interacting many-electron system with localized single-particle states, *Ann. Phys. (N.Y.)* **321**, 1126 (2006).
- [23] J. Moix and J. Cao, Coherent quantum transport in disordered systems: I. The influence of dephasing on the transport properties and absorption spectra on one-dimensional systems, *New J. Phys.* **15**, 085010 (2013).
- [24] R. Nandkishore and D. A. Huse, Many-body localization and thermalization in quantum statistical mechanics, *Annu. Rev. Condens. Matter Phys.* **6**, 15 (2015).
- [25] D. Jaksch, C. Bruder, J. I. Cirac, C. W. Gardiner, and P. Zoller, Cold Bosonic Atoms in Optical Lattices, *Phys. Rev. Lett.* **81**, 3108 (1998).
- [26] M. Greiner, O. Mandel, T. Esslinger, T. W. Hansch, and I. Bloch, Quantum phase transition from a superfluid to a Mott insulator in a gas of ultracold atoms, *Nature (London)* **415**, 39 (2002).
- [27] I. Bloch, J. Dalibard, and W. Zwerger, Many-body physics with ultracold gases, *Rev. Mod. Phys.* **80**, 885 (2008).

- [28] L. Sanchez-Palencia and M. Lewenstein, Disordered quantum gases under control, *Nat. Phys.* **6**, 22 (2010).
- [29] M. Rigol, V. Dunjko, and M. Olshanii, Thermalization and its mechanism for generic isolated quantum systems, *Nature (London)* **452**, 854 (2008).
- [30] D. C. McKay and B. DeMarco, Cooling in strongly correlated optical lattices: Prospects and challenges, *Rep. Prog. Phys.* **74**, 054401 (2011).
- [31] J. Lux, J. Muller, A. Mitra, and A. Rosch, Hydrodynamic long-time tails after a quantum quench, *Phys. Rev. A* **89**, 053608 (2014).
- [32] U. Schneider, L. Hackermueller, J. P. Ronzheimer, S. Will, S. Braun, T. Best, and I. Bloch, Fermionic transport and out-of-equilibrium dynamics in a homogeneous Hubbard model with ultracold atoms, *Nat. Phys.* **8**, 213 (2012).
- [33] V. Oganesyan and D. A. Huse, Localization of interacting fermions at high temperature, *Phys. Rev. B* **75**, 155111 (2007).
- [34] S. Q. Zhou and D. M. Ceperley, Construction of localized wave functions for a disordered optical lattice and analysis of the resulting Hubbard model parameters, *Phys. Rev. A* **81**, 013402 (2010).
- [35] Y. P. Chen, J. Hitchcock, D. Dries, M. Junker, C. Welford, and R. G. Hulet, Phase coherence and superfluid-insulator transition in a disordered Bose-Einstein condensate, *Phys. Rev. A* **77**, 033632 (2008).
- [36] M. White, M. Pasienski, D. McKay, S. Q. Zhou, D. Ceperley, and B. DeMarco, Strongly Interacting Bosons in a Disordered Optical Lattice, *Phys. Rev. Lett.* **102**, 055301 (2009).
- [37] M. Pasienski, D. McKay, M. White, and B. DeMarco, A disordered insulator in an optical lattice, *Nat. Phys.* **6**, 677 (2010).
- [38] B. Gadway, D. Pertot, J. Reeves, M. Vogt, and D. Schneble, Glassy Behavior in a Binary Atomic Mixture, *Phys. Rev. Lett.* **107**, 145306 (2011).
- [39] M. C. Beeler, M. E. W. Reed, T. Hong, and S. L. Rolston, Disorder-driven loss of phase coherence in a quasi-2D cold atom system, *New J. Phys.* **14**, 073024 (2012).
- [40] J.-P. Brantut, J. Meineke, D. Stadler, S. Krinner, and T. Esslinger, Conduction of ultracold fermions through a mesoscopic channel, *Science* **337**, 1069 (2012).
- [41] L. Tanzi, E. Lucioni, S. Chaudhuri, L. Gori, A. Kumar, C. D'Errico, M. Inguscio, and G. Modugno, Transport of a Bose Gas in 1D Disordered Lattices at the Fluid-Insulator Transition, *Phys. Rev. Lett.* **111**, 115301 (2013).
- [42] S. Krinner, D. Stadler, J. Meineke, J. P. Brantut, and T. Esslinger, Superfluidity with Disorder in a Thin Film of Quantum Gas, *Phys. Rev. Lett.* **110**, 100601 (2013).
- [43] S. S. Kondov, W. R. McGehee, W. Xu, and B. DeMarco, Disorder-Induced Localization in a Strongly Correlated Atomic Hubbard Gas, *Phys. Rev. Lett.* **114**, 083002 (2015).
- [44] R. Jordens, N. Strohmaier, K. Guenther, H. Moritz, and T. Esslinger, A Mott insulator of fermionic atoms in an optical lattice, *Nature (London)* **455**, 204 (2008).
- [45] U. Schneider, L. Hackermueller, S. Will, Th. Best, I. Bloch, T. A. Costi, R. W. Helmes, D. Rasch, and A. Rosch, Metallic and insulating phases of repulsively interacting fermions in a 3D optical lattice, *Science* **322**, 1520 (2008).
- [46] R. Jordens, L. Tarruell, D. Greif, T. Uehlinger, N. Strohmaier, H. Moritz, T. Esslinger, L. De Leo, C. Kollath, A. Georges, V. Scarola, L. Pollet, E. Burovski, E. Kozik, and M. Troyer, Quantitative Determination of Temperature in the Approach to Magnetic Order of Ultracold Fermions in an Optical Lattice, *Phys. Rev. Lett.* **104**, 180401 (2010).
- [47] J. Hubbard, Electron correlations in narrow energy bands, *Proc. R. Soc. London, Ser. A* **276**, 238 (1963).
- [48] R. Staudt, M. Dzierzawa, and A. Muramatsu, Phase diagram of the three-dimensional Hubbard model at half filling, *Eur. Phys. J. B* **17**, 411 (2000).
- [49] S. Fuchs, E. Gull, L. Pollet, E. Burovski, E. Kozik, T. Pruschke, and M. Troyer, Thermodynamics of the 3D Hubbard Model on Approaching the Neel Transition, *Phys. Rev. Lett.* **106**, 030401 (2011).
- [50] T. Paiva, Y. L. Loh, M. Randeria, R. T. Scalettar, and N. Trivedi, Fermions in 3D Optical Lattices: Cooling Protocol to Obtain Antiferromagnetism, *Phys. Rev. Lett.* **107**, 086401 (2011).
- [51] E. Kozik, E. Burovski, V. W. Scarola, and M. Troyer, Néel temperature and thermodynamics of the half-filled three-dimensional Hubbard model by diagrammatic determinant Monte Carlo, *Phys. Rev. B* **87**, 205102 (2013).
- [52] R. A. Hart, P. M. Duarte, T. Yang, X. Liu, T. Paiva, E. Khatami, R. T. Scalettar, N. Trivedi, D. A. Huse, and R. G. Hulet, Observation of antiferromagnetic correlations in the Hubbard model with ultracold atoms, *Nature (London)* **519**, 211 (2015).
- [53] A. Dirks, K. Mikelsons, H. R. Krishnamurthy, and J. K. Freericks, Simulation of inhomogeneous distributions of ultracold atoms in an optical lattice via a massively parallel implementation of nonequilibrium strong-coupling perturbation theory, *Phys. Rev. E* **89**, 023306 (2014).
- [54] D. Penn, Stability theory of the magnetic phases for a simple model of the transition metals, *Phys. Rev.* **142**, 350 (1966).
- [55] F. Gebhard, *The Mott Metal-Insulator Transition* (Springer, Berlin, 1997).
- [56] N. Strohmaier, D. Greif, R. Jordens, L. Tarruell, H. Moritz, T. Esslinger, R. Sensarma, D. Pekker, E. Altman, and E. Demler, Observation of Elastic Doubloon Decay in the Fermi-Hubbard Model, *Phys. Rev. Lett.* **104**, 080401 (2010).
- [57] R. Sensarma, D. Pekker, E. Altman, E. Demler, N. Strohmaier, D. Greif, R. Jordens, L. Tarruell, H. Moritz, and T. Esslinger, Lifetime of double occupancies in the Fermi-Hubbard model, *Phys. Rev. B* **82**, 224302 (2010).
- [58] B. Bulka, M. Schreiber, and B. Kramer, Localization, quantum interference, and the metal-insulator transition, *Z. Phys. B* **66**, 21 (1987).
- [59] J. Oitmaa, C. Hamer, and W. Zheng, *Series Expansion Methods for Strongly Interacting Lattice Models* (Cambridge University Press, Cambridge, 2006).
- [60] V. W. Scarola, L. Pollet, J. Oitmaa, and M. Troyer, Discerning Incompressible and Compressible Phases of Cold Atoms in Optical Lattices, *Phys. Rev. Lett.* **102**, 135302 (2009).
- [61] L. De Leo, J. S. Bernier, C. Kollath, A. Georges, and V. W. Scarola, Thermodynamics of the three-dimensional Hubbard model: Implications for cooling cold atomic gases in optical lattices, *Phys. Rev. A* **83**, 023606 (2011).
- [62] M. Schreiber, S. S. Hodgman, P. Bordia, H. P. Luschen, M. H. Fischer, R. Vosk, E. Altman, U. Schneider, and I. Bloch, Observation of many-body localization of interacting fermions in a quasi-random optical lattice, *Science* **349**, 842 (2015).